

Article

Switchable Dual-Wavelength Thulium-Doped Fiber Laser Based on Polarization-Maintaining Fiber Bragg Grating and Compound Cavity Filter

Xiangdong Wang¹, Fengping Yan^{1,*}, Hao Guo¹, Wei Wang², Dandan Yang¹, Pengfei Wang¹, Ting Li³, Chenhao Yu¹, Kazuo Kumamoto⁴  and Yuping Suo⁵

¹ School of Electronic and Information Engineering, Beijing Jiaotong University, Beijing 100044, China; 21111017@bjtu.edu.cn (X.W.); 22110015@bjtu.edu.cn (H.G.); 21111013@bjtu.edu.cn (D.Y.); 19111040@bjtu.edu.cn (P.W.); 20111014@bjtu.edu.cn (C.Y.)

² Institute of Optical Information, Key Laboratory of Luminescence and Optical Information, Ministry of Education, School of Physical Science and Engineering, Beijing Jiaotong University, Beijing 100044, China; 15111006@bjtu.edu.cn

³ School of Physical Science and Engineering, Beijing Jiaotong University, Beijing 100044, China; 10159@bjtu.edu.cn

⁴ Department of Electronics, Information and Communication Engineering, Osaka Institute of Technology, Osaka 535-8585, Japan; kazuo.kumamoto@oit.ac.jp

⁵ Shanxi Provincial People's Hospital, Shanxi Medical University, Taiyuan 030012, China; yuping_suo@163.com

* Correspondence: fpyan@bjtu.edu.cn

Abstract: This paper presents experimental evidence regarding a novel switchable dual-wavelength thulium-doped fiber laser (TDFL). Wavelength switching is achieved by combining a polarization-maintaining fiber Bragg grating (PM-FBG) with a polarization controller (PC). The three-coupler double-ring compound cavity (TC-DRC) structure, acting as a mode-selection filter, is designed to select a single longitudinal mode (SLM) from the dense longitudinal modes. This paper introduces the design and fabrication method of the TC-DRC filter and analyzes, in detail, the mechanism for SLM selection. The experimental results demonstrate that the designed filter exhibits excellent performance. By adjusting the PC, the TDFL achieves stable SLM operation at the wavelengths of 1940.54 nm and 1941.06 nm, respectively. The optical signal-to-noise ratio (OSNR) is superior to 65 dB. When the TDFL is tested at room temperature, there is no significant wavelength drift, and power fluctuations are less than 1.5 dB. The operation of the SLM is verified through the self-heterodyne method, and the laser maintains stable SLM states for both wavelengths after continuous operation for an hour. Furthermore, based on the phase noise demodulation method, the linewidths of both wavelengths are measured to be less than 10 kHz at the integration time of 0.001 s.

Keywords: single-longitudinal-mode; thulium-doped fiber laser; compound ring cavity filter; polarization-maintaining fiber Bragg grating



Citation: Wang, X.; Yan, F.; Guo, H.; Wang, W.; Yang, D.; Wang, P.; Li, T.; Yu, C.; Kumamoto, K.; Suo, Y. Switchable Dual-Wavelength Thulium-Doped Fiber Laser Based on Polarization-Maintaining Fiber Bragg Grating and Compound Cavity Filter.

Photonics **2024**, *11*, 360. <https://doi.org/10.3390/photonics11040360>

Received: 4 March 2024

Revised: 25 March 2024

Accepted: 10 April 2024

Published: 12 April 2024



Copyright: © 2024 by the authors. Licensee MDPI, Basel, Switzerland. This article is an open access article distributed under the terms and conditions of the Creative Commons Attribution (CC BY) license (<https://creativecommons.org/licenses/by/4.0/>).

1. Introduction

Thulium ions possess multiple excitation and emission energy levels, enabling the realization of a wide wavelength range for laser output [1,2]. The operational principle of a thulium-doped fiber laser (TDFL) involves exciting thulium ions to higher energy levels through either electrical heating or optical pumping, leading to transitions between lower and upper energy levels and the emission of laser light [3]. With technological advancements, TDFLs have been adopted in various fields. In telecommunication, they can be used for signal amplification in optical communication systems and as light sources in optical fiber sensors [4–6]. In laser processing, TDFLs find applications in cutting, welding, hole drilling, and other machining processes [7–9]. In the medical field, these lasers are employed in laser surgery, skin treatments, and ophthalmic surgeries [10–18]. They also

offer advantages such as a broad wavelength range (1660–2200 nm), high efficiency, and versatility across multiple application domains, making them a significant area of research in recent years.

The single-longitudinal-mode (SLM) TDFL, due to its excellent SLM oscillation characteristics and narrow linewidth, is a preferred light source for various applications, including optical measurement, coherent optical communication, and optical fiber sensing. Given the demand for ultra-high spatial resolution in these fields, we have created and employed various narrowband filters to optimize the longitudinal mode interval. Compared to conventional distributed feedback (DFB) fiber lasers and distributed Bragg reflector (DBR) fiber lasers [19,20], the SLM thulium-doped ring-cavity fiber laser offers advantages such as high output power and no spatial hole burning [21]. However, the overall cavity length of the ring cavity is relatively long, leading to small longitudinal mode spacing. Appropriate filters need to be designed in the cavity to increase the effective longitudinal mode spacing further and reduce the longitudinal density. Due to the stringent requirements of ultra-narrowband filter bandwidths, the manufacturing process becomes more complex. Therefore, achieving SLM operation using only polarization-maintaining fiber Bragg grating (PM-FBG) is challenging. While using a saturable absorber (SA) for SLM operation is an option, it requires a sufficiently long length, leading to lower slope efficiency [22]. Critical filtering components are also relatively scarce and expensive in the 2 μm band. Thus, manufacturing a sub-ring cavity filter, such as a multi-ring compound ring cavity filter, becomes an easily implementable, cost-effective, and flexible solution. A multi-ring compound cavity filter typically consists of a main cavity providing gain combined with one or more passive sub-cavities filters. The passive sub-ring cavity filter usually comprises one or more 2×2 optical couplers (OCs) that serve as filters for longitudinal mode selection in the main cavity. Based on the above analysis, a combination of PM-FBG and a three-coupler double-ring compound (TC-DRC) cavity filter is employed to achieve mode selection within the main ring cavity.

In addition, multi-wavelength lasers with switchable characteristics have broad applications in wavelength-division multiplexing systems, microwave signal generation, high-resolution spectrometers, optical fiber sensing, and other fields. In recent years, various wavelength-tuning techniques have been reported, including multi-wavelength lasers based on all-fiber Mach–Zehnder interferometers with 3 dB OCs [23]; introducing polarization-dependent components such as few-mode or multi-mode fiber gratings to weaken the competition among different wavelengths through polarization hole burning effects [24], achieving multi-wavelength output; and utilizing the intensity-dependent balanced effect of nonlinear polarization rotation to achieve multiple-wavelength lasing [25]. Among these methods, the PM-FBG allows for advanced knowledge of the reflection wavelength and bandwidth positions, facilitating parameter selection and numerical simulation. By adjusting the state of the polarization controller (PC), the birefringence state inside the cavity can be changed, causing variations in the intensity of the two reflection peaks of PM-FBG. Compared to other methods, a wavelength-switchable dual-wavelength TDFL designed with PM-FBG exhibits advantages such as a simple structure, stable output, and ease of control.

In this work, a dual-wavelength tunable SLM TDFL is proposed and demonstrated experimentally. The TDFL achieves SLM operation using a laboratory-made PM-FBG and a TC-DRC cavity filter. Firstly, the transmission spectrum of the PM-FBG is measured, and a numerical simulation analysis of the TC-DRC cavity filter is conducted, laying the foundation for further experiments. The basic principles and mode-selection mechanism of achieving SLM inside the ring cavity are analyzed. Subsequently, the output optical spectra, wavelength drift, and power fluctuations of the two wavelengths are measured at room temperature over 60 min, along with the spectra used to confirm SLM operation. Finally, based on a phase noise demodulation method, the laser linewidth measurement system is employed to measure the linewidth of the two output wavelengths at different integration times. The experimental results indicate that the TDFL exhibits stable output performance.

2. Experimental Instrument and Principles

As shown in Figure 1a, a 793 nm laser diode (LD) (K793DA3RN12.00W, BWT Beijing Ltd., Beijing, China) with a maximum output power of 12 W was employed to provide pump energy to the gain fiber through a 790/2000 nm coupler (FC, Light Comm Technology). The gain fiber was a 4.5 m long Tm^{3+} -doped double-clad fiber with a core/cladding diameter of 10/130 μm and a numerical aperture (NA) of 0.15 (Nufern, thulium-doped, TDF). The absorption coefficient of the thulium-doped fiber at 793 nm was 4.5 dB/m. The other end of the thulium-doped fiber (TDFL) was connected to port 1 of the circulator (CIR), ensuring unidirectional laser operation within the cavity. Port 2 of the CIR was connected to a PM-FBG for initial wavelength selection. To avoid the impact of reflections from the free-end pigtail of the PM-FBG, the pigtail fiber of the PM-FBG was spliced to a FC/APC connector. The PM-FBG, serving as a dual-channel filter, was fabricated in a polarization-preserving fiber using the phase mask method. Compared with a three-ring PC, a drop-in PC with low loss in the 2 μm band was selected to adjust the polarization state. A TC-DRC cavity filter implemented the mode selection mechanism, with the reflected light signal from the PM-FBG entering the passive TC-DRC cavity filter through port 3 of the CIR. The TC-DRC cavity filter, as shown in Figure 1b, consisted of three OCs (OC1, OC2, and OC3): OC1 was a 90:10 2×2 coupler, while OC2 and OC3 were 50:50 2×2 homemade couplers. Additionally, $L_1 + L_4 + L_2$ formed the large ring (Ring-1), and $L_2 + L_3$ composed the small ring (Ring-2), where $L_1 = L_2 = L_4 = 1$ m and $L_3 = 2.05$ m. The final 1×2 OC outputted 10% of the laser from the main cavity. The total cavity length of the constructed laser was ~ 16.48 m, resulting in longitudinal mode spacing of ~ 12.7 MHz in the main cavity.

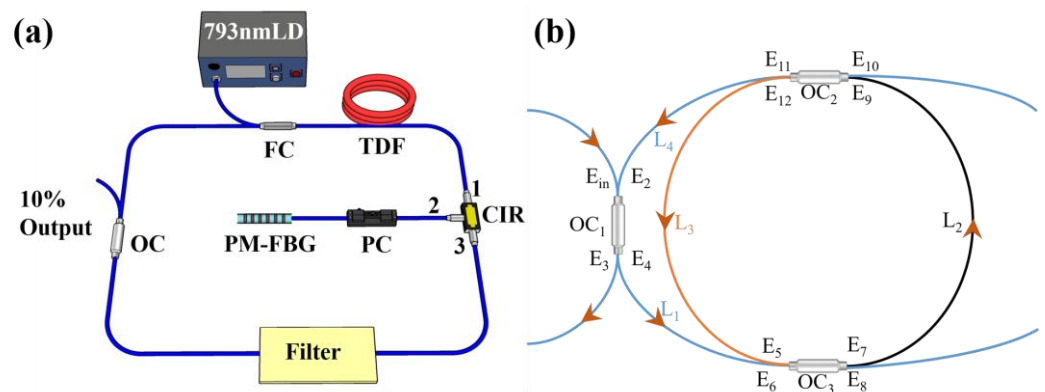


Figure 1. (a) Configuration diagram of the proposed switchable dual-wavelength TDFL. (b) Schematic diagram of the proposed TC-DRC cavity filter. E_{in} – E_{12} represent the electric field amplitudes at the ports of OC; L_1 – L_4 are the lengths of the optical fibers.

The PM-FBG has high birefringence, and its transmission modes are the two fundamental modes with mutually perpendicular polarization directions. It has two optical axes, so the refractive indices for the two polarization directions differ. The limited refractive indices in the slow and fast axis directions of the polarization-maintaining fiber are denoted as n_{effx} and n_{effy} , respectively. Reflection occurs on both optical axes due to the grating, and the peak reflection wavelengths of the two spectra (λ_x and λ_y) satisfy the following grating peak wavelength formula:

$$\lambda_x = 2n_{effx}\Lambda \quad (1)$$

$$\lambda_y = 2n_{effy}\Lambda \quad (2)$$

where Λ is the grating period. The separation ($\Delta\lambda_B$) between the two reflection wavelengths is given by the following:

$$L_B = \lambda / (n_{effx} - n_{effy}) \quad (3)$$

$$\Delta\lambda_B = 2\Lambda \Delta n_{eff} \quad (4)$$

In the given expressions, L_B denotes the beat length of the polarization-maintaining fiber, λ is the operating wavelength, $\Delta\lambda_B$ represents the difference between the two Bragg wavelengths of the grating, and Λ is the grating period [26,27].

In this experiment, with $L_B = 2.7$ mm, the wavelength spacing between the two orthogonally polarized modes reflected by the grating was approximately 0.57 nm. Panda polarization-maintaining fiber was used to inscribe using the phase mask method with a length of 2 cm. The optical spectra of the PM-FBG were measured using an optical spectrum analyzer (OSA, Yokogawa, AQ6375B). The transmission spectra of the two wavelengths are shown in Figure 2, measured by the OSA with a resolution of 0.05 nm. The transmission depths at 1940.55 nm and 1941.07 nm were 11.02 dB and 11.65 dB, corresponding to reflectivity of approximately 91% and 93%, respectively. The 3 dB bandwidth of the reflection peak was 0.097 nm, corresponding to a frequency range of about 7.56 GHz.

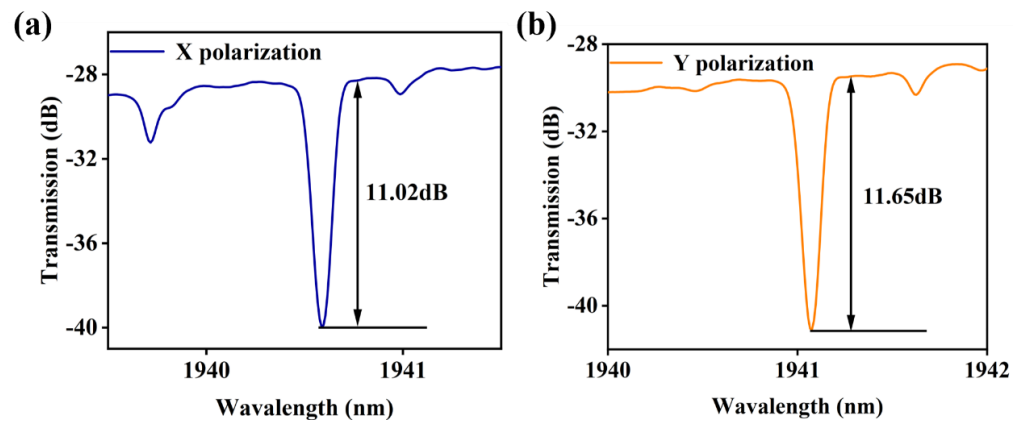


Figure 2. Transmission spectra of PM-FBG under (a) X-polarization and (b) Y-polarization.

3. SLM of Principle

Figure 1b shows the schematic diagram of the proposed passive TC-DRC cavity filter, consisting of three OCs (OC1, OC2, and OC3) forming two sub-rings. The working conditions of the laser inside the sub-cavity were analyzed using the signal flowchart initially proposed by Mason [28,29]. Here, E_1-E_{12} represent the electric field amplitudes at the optical ports of the couplers, L_1-L_4 are the lengths of the optical fibers, $\kappa_i (i = 1, 2, 3, 4)$ is the cross-coupling ratio, $\gamma_i (i = 1, 2, 3, 4)$ is the insertion losses of the optical fibers, α is the fiber loss coefficient, δ is the splice and cleave loss, $\beta = 2\pi n_{eff} / \lambda$ is the propagation constant of light, n_{eff} is the effective refractive index, and λ is the wavelength. The signal flowchart and laser transmission for the sub-cavity consisting of 12 nodes are shown in Figure 3.

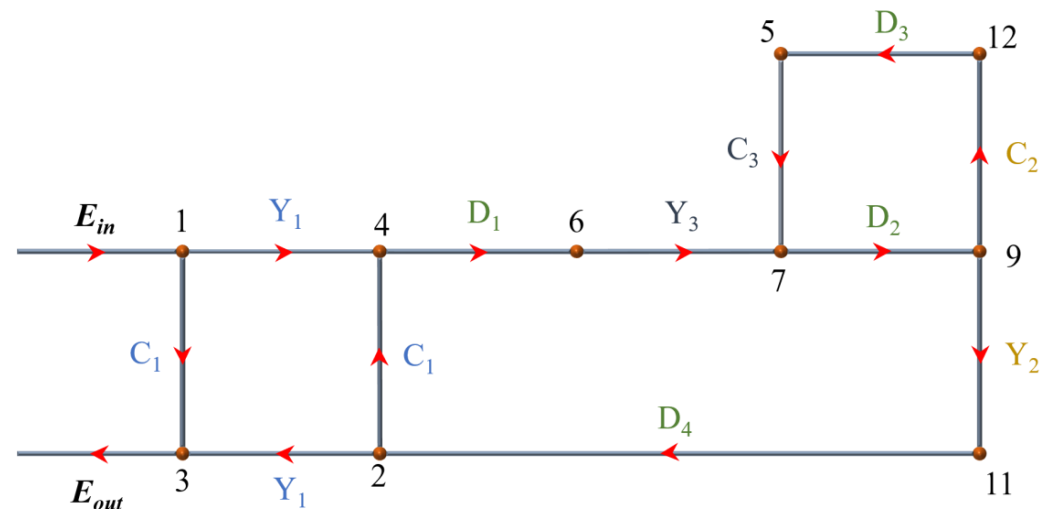


Figure 3. Signal flowchart of the passive TC-DRC cavity filter.

As shown in Figure 3, the transmission path gain coefficient C_i ($i = 1, 2, 3, 4$) for OCs is defined as follows:

$$C_i = \sqrt{1 - \kappa_i} \sqrt{1 - \gamma_i} (i = 1, 2, 3, 4) \tag{5}$$

The coupling path gain coefficient Y_i for OC1 is defined as follows:

$$Y_i = i\sqrt{\kappa_i} \sqrt{1 - \gamma_i} (i = 1, 2, 3, 4) \tag{6}$$

The transmission path gain coefficient D_i for the optical fiber is the following:

$$D_i = \sqrt{1 - \delta e^{(-\alpha + j\beta)L_i}} (i = 1, 2, 3, 4) \tag{7}$$

$$\begin{aligned} E_3 &= C_1 E_1 + Y_1 E_2 \\ E_4 &= C_1 E_2 + Y_1 E_1 \\ E_6 &= D_1 E_4 \\ E_7 &= C_2 E_5 + Y_2 E_6 \\ E_9 &= D_2 E_7 \\ E_{11} &= C_3 E_{10} + Y_3 E_9 \\ E_{12} &= C_3 E_9 + Y_3 E_{10} \\ E_5 &= D_3 E_{12} \\ E_2 &= D_4 E_{11} \end{aligned} \tag{8}$$

As shown in Figure 1b, when the incident light passed through the TC-DRC cavity filter for the first time, the incident light intensity at port 2 of OC1, port 5 of OC3, and port 10 of OC2 were all equal to 0 ($E_2 = 0, E_5 = 0,$ and $E_{10} = 0$). Equation (8) can be decomposed into matrix form for the ease of solving it, as follows:

$$M = \begin{pmatrix} 1 & 0 & 0 & 0 & 0 & 0 & 0 & 0 & 0 & 0 & 0 & 0 \\ 0 & -1 & 0 & 0 & 0 & 0 & 0 & 0 & 0 & 0 & D_4 & 0 \\ C_1 & Y_1 & 0 & 0 & 0 & 0 & 0 & 0 & 0 & 0 & 0 & 0 \\ Y_1 & C_1 & 0 & -1 & 0 & 0 & 0 & 0 & 0 & 0 & 0 & 0 \\ 0 & 0 & 0 & 0 & -1 & 0 & 0 & 0 & 0 & 0 & 0 & D_3 \\ 0 & 0 & 0 & D_1 & 0 & -1 & 0 & 0 & 0 & 0 & 0 & 0 \\ 0 & 0 & 0 & 0 & C_3 & Y_3 & -1 & 0 & 0 & 0 & 0 & 0 \\ 0 & 0 & 0 & 0 & Y_3 & C_3 & 0 & -1 & 0 & 0 & 0 & 0 \\ 0 & 0 & 0 & 0 & 0 & 0 & D_2 & 0 & -1 & 0 & 0 & 0 \\ 0 & 0 & 0 & 0 & 0 & 0 & 0 & 0 & 0 & -1 & 0 & 0 \\ 0 & 0 & 0 & 0 & 0 & 0 & 0 & 0 & Y_2 & C_2 & -1 & 0 \\ 0 & 0 & 0 & 0 & 0 & 0 & 0 & 0 & C_2 & Y_2 & 0 & -1 \end{pmatrix}, E = \begin{pmatrix} E_1 \\ E_2 \\ E_3 \\ E_4 \\ E_5 \\ E_6 \\ E_7 \\ E_8 \\ E_9 \\ E_{10} \\ E_{11} \\ E_{12} \end{pmatrix}, B = \begin{pmatrix} 1 \\ 0 \\ 0 \\ 0 \\ 0 \\ 0 \\ 0 \\ 0 \\ 0 \\ 0 \\ 0 \\ 0 \end{pmatrix}, ME = B \tag{9}$$

Numerical solutions can be obtained using the built-in algorithm of the program.

$$E = M^{-1}B \tag{10}$$

The transmittance of the TC-DRC filter can be expressed as follows:

$$T = \left(\frac{E_3}{E_1}\right) \cdot \left(\frac{E_3}{E_1}\right)^* \tag{11}$$

Based on the above analysis, MATLAB can be used for the transmission spectrum of the TC-DRC cavity filter. The 3 dB reflection bandwidth of both channels of PM-FBG was less than 0.097 nm, with main cavity longitudinal mode spacing of 12.7 MHz, where using the TC-DRC cavity filter as the mode-selection mechanism achieves the SLM operation of the laser. Two principles need to be satisfied. First, the effective free spectral range (FSR) of the TC-DRC cavity filter should be greater than 0.5 times and less than 1 times the bandwidth of PM-FBG. Secondly, the longitudinal mode spacing of the main ring cavity should be greater than 0.5 times and less than 1 times the full width at half maximum (FWHM) of the TC-DRC cavity filter’s main resonance peak. Only an SLM can be selected from the dense modes within the grating bandwidth through this method. While designing

TC-DRC parameters, the fiber loss coefficient, fusion loss, effective refractive index of single-mode fiber (SMF), and the insertion loss of OCs are constants. By changing the lengths L_i of the sub-ring cavities and the coupling ratio of OCs, the transmission performance of the TC-DRC cavity filter can be optimized. This primarily affects the Q value of the laser cavity, which is the laser cavity's capacity for storing energy. In contrast, the cavity length L_i determines the FSR of the TC-DRC filter. The formula for calculating FSR is as follows:

$$FSR = \frac{c}{n_{eff}L_{cavity}} \tag{12}$$

In this formula, c represents the speed of light in a vacuum. As the above equation indicates, sub-cavity FSR is inversely proportional to L .

As shown in Figure 4, the envelope of FSR of the TC-DRC filter was 4.08 GHz, and the measured peak transmission bandwidth was approximately 22.3 MHz, about 1.75 times the longitudinal mode spacing of the main cavity. Theoretically, the proposed TC-DRC cavity filter in the 16.48 m cavity length TDFL exhibited excellent SLM selection capability.

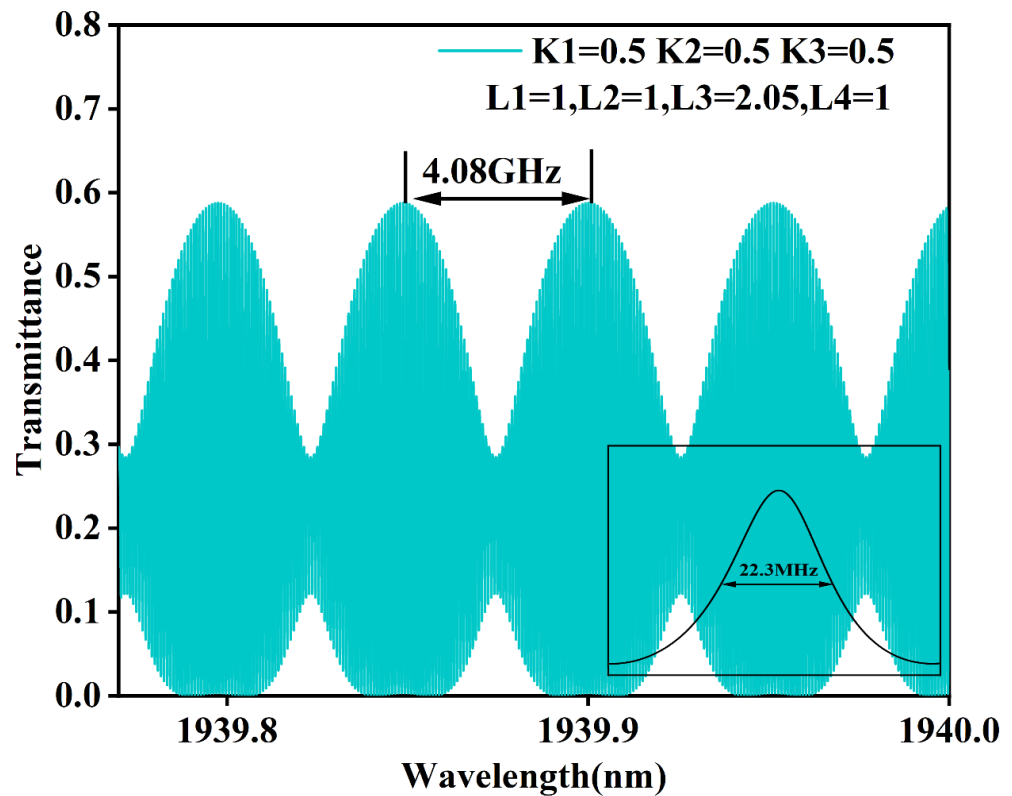


Figure 4. Simulation results of the proposed passive TC-DRC cavity filter.

4. Experimental Results and Discussion

This experiment was conducted at normal room temperature, and the TDFL system was placed on an extremely stable optical platform. The laser threshold of TDFL was 2.6 W. Initially, an OSA was used to record the spectra of single-wavelength operation, as shown in Figure 5a,b, with center wavelengths of 1940.54 nm and 1941.06 nm, which coincided with the peak reflection wavelengths of PM-FBG. The optical signal-to-noise ratios (OSNRs) for the output wavelengths were 65 dB and 67 dB. To verify the stability of the output wavelengths, ten repeated OSA scans were performed for each wavelength over a time span of more than an hour (~60 min) with intervals of ~6 min, as shown in Figure 5c,d. Additionally, Table 1 presents the wavelength drift and power fluctuations of the laser output within 60 min, indicating wavelength drifts less than 0.03 nm (below the resolution of OSA) and power fluctuations below 1.5 dB. These results demonstrate that the proposed TDFL exhibits excellent stability.

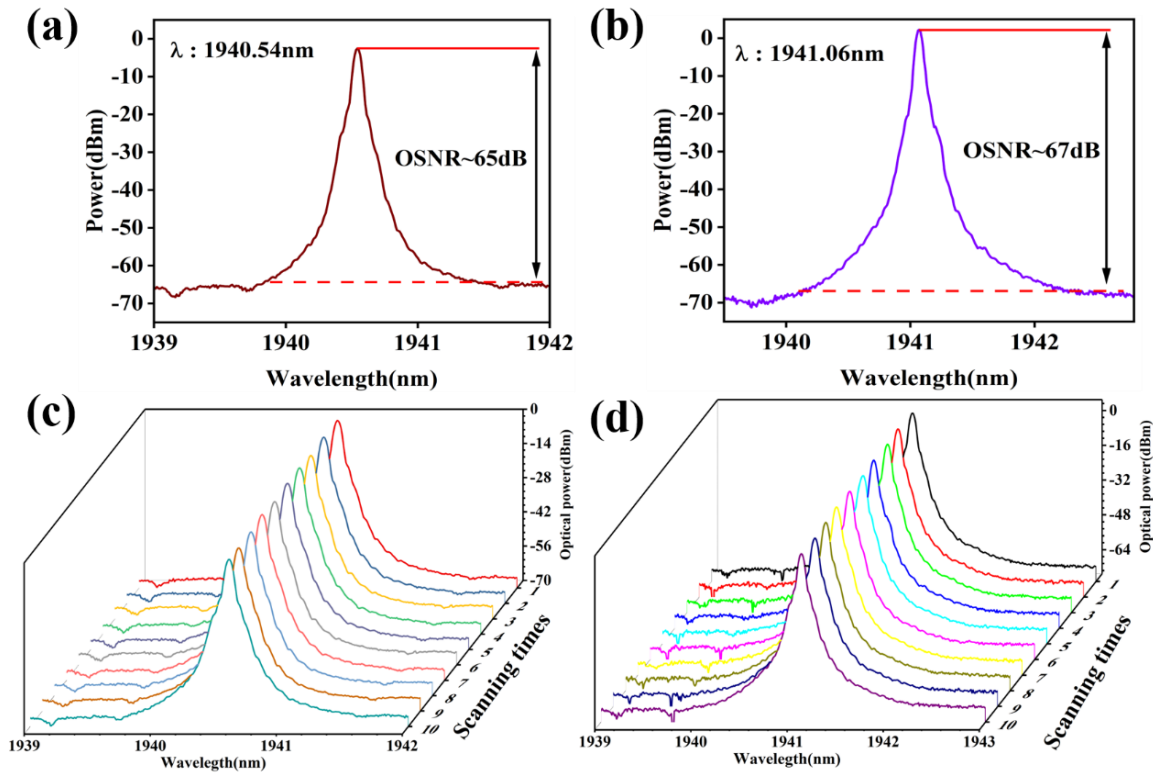


Figure 5. Laser spectra corresponding to PM-FBG, with wavelengths of (a) 1940.54 nm and (b) 1941.06 nm. (c,d) Stable spectra obtained from 10 consecutive scans with a 6 min interval.

Table 1. Wavelength drift and power fluctuations over 60 minutes.

Wavelength (nm)	Wavelength Drift (nm)	Power Fluctuations (dB)
1940.54	0.03	0.8
1941.06	0.02	1.3

The radio frequency (RF) spectrum of the laser was detected using a 12.5 GHz photodetector (PD, ET-5000F) and a 26.5 GHz signal analyzer (Keysight, N9020A). The RF spectrum scan range was set to 0–100 MHz with a resolution bandwidth (RBW) of 1 MHz. Figure 6a,c show the RF spectra for the laser output wavelengths of 1940.54 nm and 1941.06 nm, respectively. Figure 6b,d present the RF spectra for the two wavelengths measured every 6 min over 60 min, indicating that the proposed TDFL maintained stable SLM operation at both output wavelengths.

Figure 7 shows the laboratory-made linewidth measurement system in the laboratory based on the phase noise demodulation method [30]. It employed a non-balanced Michelson interferometer (MI) linewidth measurement system consisting of a 3×3 coupler and two Faraday rotation mirrors (FRMs) to obtain the noise information. Compared to traditional linewidth measurement methods that use super-long delay lines, using a 50 m long SMF as the delay line helps reduce losses. The two FRMs reflected light with a time difference due to different transmission distances, and two identical PDs detected this light. The collected data were then processed to calculate the power spectral density (PSD) of the instantaneous phase and frequency fluctuations of the laser. Using the β -separation line method, the linewidths of four output wavelengths were measured at different integration times (0.001 s, 0.005 s, 0.01 s, 0.05 s, 0.1 s, 0.5 s, and 1 s). This linewidth measurement method increases linewidth with longer measurement times due to the $1/f$ noise in the PSD of frequency fluctuations. The measurements were conducted in a relatively quiet environment since linewidth is affected by temperature and vibration. The PSD of the frequency noise spectrum and linewidth of the laser, obtained through measurement and

analysis, is shown in Figure 8. The linewidth increased with increasing integration time. Table 2 provides the measured linewidth results for the output wavelengths, and it can be concluded that the linewidths for the two wavelengths were 7.8 kHz and 8.06 kHz at 0.001 s, respectively.

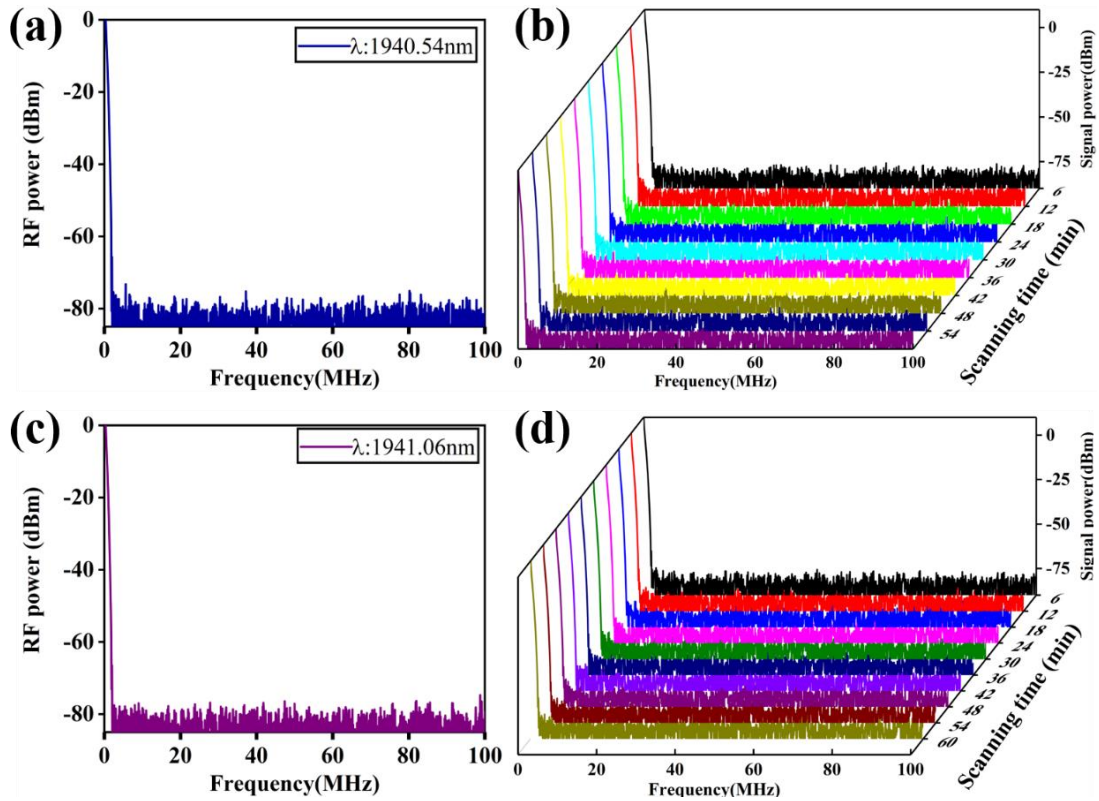


Figure 6. Laser beat frequency results in the presence of the passive TC–DRC cavity filter with a frequency range of 0 to 100 MHz. The laser output wavelengths from the self-heterodyne method are (a) 1940.54 nm and (b) 1941.06 nm. (c,d) Beat frequency results measured at intervals of 6 min over a continuous one-hour period.

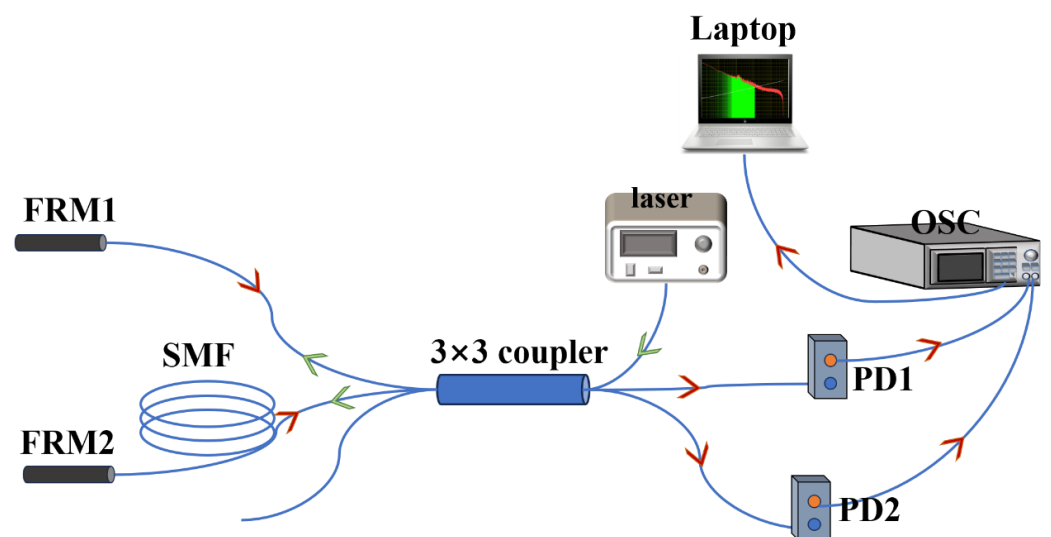


Figure 7. Configuration of the linewidth measurement system. FRM: Faraday rotation mirror, PD: photodetector, CH: channel.

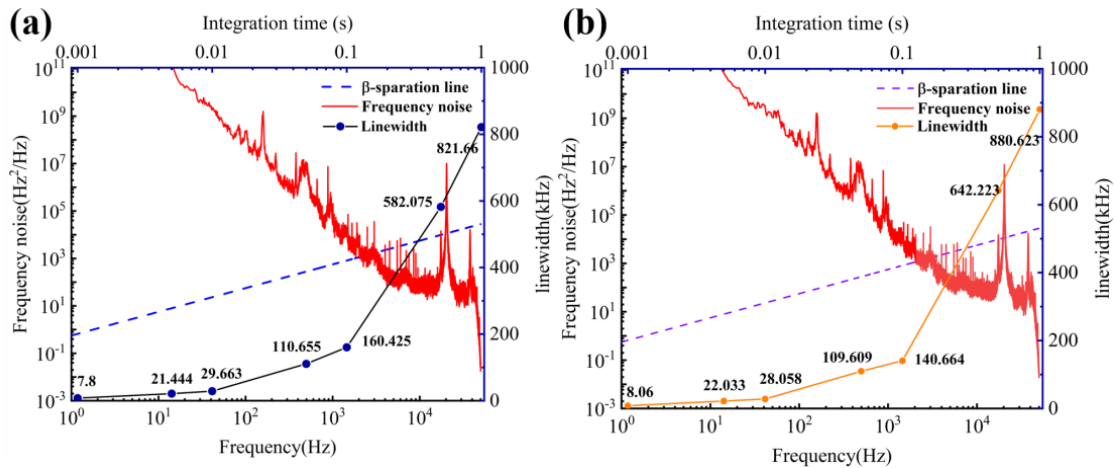


Figure 8. Frequency noise PSD of the SLM laser at (a) 1941.06 nm and (b) 1940.54 nm.

Table 2. Laser linewidth measured at two wavelengths at different times.

<i>T</i> (s)	0.001	0.005	0.01	0.1	1
Linewidth at the wavelength 1940.54 nm (kHz)	7.8	21.444	28.663	160.425	821.663
Linewidth at the wavelength 1941.06 nm (kHz)	8.06	22.033	28.058	140.664	880.623

5. Conclusions

A dual-wavelength tunable TDFL utilizing a PM-FBG and TC-DRC cavity filter was proposed and investigated experimentally. The PM-FBG, with a 3 dB bandwidth of ~0.097 nm, was combined with three fiber couplers in a TC-DRC structure for SLM selection. The laser operated in the SLM at different wavelengths by adjusting the PC at room temperature, achieving an OSNR greater than 65 dB. Over a continuous measurement period of 60 min, the laser exhibited a maximum wavelength drift of 0.03 nm and maximum power fluctuation of 1.5 dB, consistently maintaining a stable SLM output. The linewidth of the output laser, measured using a laboratory-made linewidth measurement system, was less than 10 kHz, comparable to SLM lasers reported in this wavelength range. This laser could be an ideal light source for spatial optical communication and optical measurement systems.

Author Contributions: Conceptualization, X.W.; methodology, F.Y.; software, H.G.; validation, W.W.; formal analysis, D.Y.; investigation, P.W.; resources, T.L.; data curation, C.Y.; writing—original draft preparation, K.K.; writing—review and editing, Y.S.; visualization, D.Y. All authors have read and agreed to the published version of the manuscript.

Funding: This work was supported by the National Key Research and Development Program of China (2021YFB2800900) and the Key Program of the National Natural Science Foundation of China (62335001).

Institutional Review Board Statement: Not applicable.

Informed Consent Statement: Not applicable.

Data Availability Statement: The data presented in this study may be available from the corresponding author upon reasonable request.

Conflicts of Interest: The authors declare no conflicts of interest.

References

1. Ter-Mikirtychev, V. *Fundamentals of Fiber Lasers and Fiber Amplifiers*; Springer: Berlin/Heidelberg, Germany, 2014; Volume 99.
2. Jackson, S.D.; King, T.A. Theoretical modeling of Tm-doped silica fiber lasers. *J. Light. Technol.* **1999**, *17*, 948. [[CrossRef](#)]
3. Moulton, P.F.; Rines, G.A.; Slobodtchikov, E.V.; Wall, K.F.; Frith, G.; Samson, B.; Carter, A.L. Tm-doped fiber lasers: Fundamentals and power scaling. *IEEE J. Sel. Top. Quantum Electron.* **2009**, *15*, 85–92. [[CrossRef](#)]
4. Qin, Q.; Li, T.; Yan, F.; Feng, T.; Sun, W.; Han, W.; Yang, D.; Wang, X.; Yu, C.; Wang, P. Demonstration of the first outdoor 2- μ m-band real-time video transmission free-space optical communication system using a self-designed single-frequency fiber laser. *J. Light. Technol.* **2023**, *41*, 5275–5283. [[CrossRef](#)]
5. Huang, C.; Tang, Y.; Li, H.; Wang, Y.; Xu, J.; Du, C. A versatile model for temperature-dependent effects in Tm-doped silica fiber lasers. *J. Light. Technol.* **2013**, *32*, 421–428. [[CrossRef](#)]
6. Kieleck, C.; Berrou, A.; Donelan, B.; Cadier, B.; Robin, T.; Eichhorn, M. 6.5 W ZnGeP 2 OPO directly pumped by a Q-switched Tm 3+-doped single-oscillator fiber laser. *Opt. Lett.* **2015**, *40*, 1101–1104. [[CrossRef](#)] [[PubMed](#)]
7. Roesner, A.; Abels, P.; Olowinsky, A.; Matsuo, N.; Hino, A. Absorber-free laser beam welding of transparent thermoplastics. In Proceedings of the International Congress on Applications of Lasers & Electro-Optics, Temecula CA, USA, 20–23 October 2008.
8. Mingareev, I.; Weirauch, F.; Olowinsky, A.; Shah, L.; Kadwani, P.; Richardson, M. Welding of polymers using a 2 μ m thulium fiber laser. *Opt. Laser Technol.* **2012**, *44*, 2095–2099. [[CrossRef](#)]
9. McComb, T.S.; Sims, R.A.; Willis, C.C.; Kadwani, P.; Shah, L.; Richardson, M. Atmospheric transmission testing using a portable, tunable, high power thulium fiber laser system. In *Conference on Lasers and Electro-Optics*; Optica Publishing Group: Washington, DC, USA, 2010; p. JThJ5.
10. Xylinas, E.; Rink, M.; Cha, E.K.; Clozel, T.; Lee, R.K.; Fajkovic, H.; Comploj, E.; Novara, G.; Margulis, V.; Raman, J.D. Impact of distal ureter management on oncologic outcomes following radical nephroureterectomy for upper tract urothelial carcinoma. *Eur. Urol.* **2014**, *65*, 210–217. [[CrossRef](#)] [[PubMed](#)]
11. Zhang, J.; Ou, Z.; Zhang, X.; He, W.; Wang, R.; Mo, M.; Chen, L.; Xu, R.; Jiang, S.; Peng, X. Holmium laser enucleation of the prostate versus thulium laser enucleation of the prostate for the treatment of large-volume prostates > 80 ml: 18-month follow-up results. *World J. Urol.* **2020**, *38*, 1555–1562. [[CrossRef](#)] [[PubMed](#)]
12. Janeczek, M.; Świdorski, J.; Czerski, A.; Żywicka, B.; Bujok, J.; Szymonowicz, M.; Bilewicz, E.; Dobrzyński, M.; Korczyński, M.; Chrószcz, A. Preliminary evaluation of thulium doped fiber laser in pig model of liver surgery. *BioMed Res. Int.* **2018**, *2018*, 3275284. [[CrossRef](#)]
13. Becker, B.; Enikeev, D.; Netsch, C.; Gross, A.J.; Laukhtina, E.; Glybochko, P.; Rapoport, L.; Herrmann, T.R.; Taratkin, M. Comparative analysis of vaporization and coagulation properties of a hybrid laser (combination of a thulium and blue diode laser) vs thulium and Ho: YAG lasers: Potential applications in endoscopic enucleation of the prostate. *J. Endourol.* **2020**, *34*, 862–867. [[CrossRef](#)]
14. Wen, J.; Ji, Z.G.; Li, H.Z. Treatment of upper tract urothelial carcinoma with ureteroscopy and thulium laser: A retrospective single center study. *BMC Cancer* **2018**, *18*, 196. [[CrossRef](#)] [[PubMed](#)]
15. Sciarra, A.; Von Heland, M.; Minisola, F.; Salciccia, S.; Cattarino, S.; Gentile, V. Thulium laser supported nephron sparing surgery for renal cell carcinoma. *J. Urol.* **2013**, *190*, 698–701. [[CrossRef](#)] [[PubMed](#)]
16. Glybochko, P.; Alyaev, Y.; Rapoport, L.; Enikeev, D.; Enikeev, M.; Sorokin, N.; Sukhanov, R.; Dymov, A.; Taratkin, M. PDD-guided thulium fiber laser en-bloc enucleation of bladder tumor. *Eur. Urol. Suppl.* **2018**, *17*, e1967. [[CrossRef](#)]
17. Chiron*, P.; Berthe, L.; Haddad, M.; Doizi, S.; Traxer, O. PD59-06 in vitro comparison of efficiency between superpulsed thulium fiber laser and HO: YAG laser for endocorporeal lithotripsy. *J. Urol.* **2019**, *201*, e1093. [[CrossRef](#)]
18. Enikeev, D.; Traxer, O.; Taratkin, M.; Okhunov, Z.; Shariat, S. A review of thulium-fiber laser in stone lithotripsy and soft tissue surgery. *Curr. Opin. Urol.* **2020**, *30*, 853–860. [[CrossRef](#)]
19. Voo, N.; Sahu, J.; Ibsen, M. 345-mW 1836-nm single-frequency DFB fiber laser MOPA. *IEEE Photonics Technol. Lett.* **2005**, *17*, 2550–2552. [[CrossRef](#)]
20. Guan, X.; Yang, C.; Qiao, T.; Lin, W.; Zhao, Q.; Tang, G.; Qian, G.; Qian, Q.; Yang, Z.; Xu, S. High-efficiency sub-watt in-band-pumped single-frequency DBR Tm 3+-doped germanate fiber laser at 1950 nm. *Opt. Express* **2018**, *26*, 6817–6825. [[CrossRef](#)]
21. Chen, X.; Deng, Z.; Yao, J. Photonic generation of microwave signal using a dual-wavelength single-longitudinal-mode fiber ring laser. *IEEE Trans. Microw. Theory Tech.* **2006**, *54*, 804–809. [[CrossRef](#)]
22. Li, Y.; Huang, L.; Gao, L.; Lan, T.; Cao, Y.; Ikechukwu, I.P.; Shi, L.; Liu, Y.; Li, F.; Zhu, T. Optically controlled tunable ultra-narrow linewidth fiber laser with Rayleigh backscattering and saturable absorption ring. *Opt. Express* **2018**, *26*, 26896–26906. [[CrossRef](#)]
23. An, H.; Lin, X.; Pun, E.; Liu, H. Multi-wavelength operation of an erbium-doped fiber ring laser using a dual-pass Mach-Zehnder comb filter. *Opt. Commun.* **1999**, *169*, 159–165. [[CrossRef](#)]
24. Lee, Y.W.; Lee, B. Wavelength-switchable erbium-doped fiber ring laser using spectral polarization-dependent loss element. *IEEE Photonics Technol. Lett.* **2003**, *15*, 795–797.
25. Zhang, Z.; Zhan, L.; Xu, K.; Wu, J.; Xia, Y.; Lin, J. Multiwavelength fiber laser with fine adjustment, based on nonlinear polarization rotation and birefringence fiber filter. *Opt. Lett.* **2008**, *33*, 324–326. [[CrossRef](#)] [[PubMed](#)]
26. Feng, S.; Xu, O.; Lu, S.; Mao, X.; Ning, T.; Jian, S. Switchable dual-wavelength erbium-doped fiber-ring laser based on one polarization maintaining fiber Bragg grating in a Sagnac loop interferometer. *Opt. Laser Technol.* **2009**, *41*, 264–267. [[CrossRef](#)]

27. Feng, S.; Xu, O.; Lu, S.; Ning, T.; Jian, S. Switchable multi-wavelength erbium-doped fiber ring laser based on cascaded polarization maintaining fiber Bragg gratings in a Sagnac loop interferometer. *Opt. Commun.* **2008**, *281*, 6006–6010. [[CrossRef](#)]
28. Mason, S.J. Feedback theory-some properties of signal flow graphs. *Proc. IRE* **1953**, *41*, 1144–1156. [[CrossRef](#)]
29. Feng, T.; Wei, D.; Bi, W.; Sun, W.; Wu, S.; Jiang, M.; Yan, F.; Suo, Y.; Yao, X.S. Wavelength-switchable ultra-narrow linewidth fiber laser enabled by a figure-8 compound-ring-cavity filter and a polarization-managed four-channel filter. *Opt. Express* **2021**, *29*, 31179–31200. [[CrossRef](#)]
30. Bai, Y.; Yan, F.; Feng, T.; Han, W.; Zhang, L.; Cheng, D.; Bai, Z.; Wen, X. Demonstration of linewidth measurement based on phase noise analysis for a single frequency fiber laser in the 2 μm band. *Laser Phys.* **2019**, *29*, 075102. [[CrossRef](#)]

Disclaimer/Publisher’s Note: The statements, opinions and data contained in all publications are solely those of the individual author(s) and contributor(s) and not of MDPI and/or the editor(s). MDPI and/or the editor(s) disclaim responsibility for any injury to people or property resulting from any ideas, methods, instructions or products referred to in the content.